Energy Conversion and Management 177 (2018) 363–375

Contents lists available at ScienceDirect

Energy Conversion and Management

journal homepage: www.elsevier.com/locate/enconman

Energy and exergy analysis of solar stills with micro/nano particles: A comparative study

Swellam W. Sharshir[a,b,c], Guilong Peng[a,d], A.H. Elsheikh[f], Elbager M.A. Edreis[g,h], Mohamed A. Eltawil[i], Talaat Abdelhamid[j], A.E. Kabeel[k], Jianfeng Zang[b,e], Nuo Yang[a,d,*]

[a] State Key Laboratory of Coal Combustion, Huazhong University of Science and Technology, Wuhan 430074, China
[b] School of Optical and Electronic Information, Huazhong University of Science and Technology, Wuhan 430074, China
[c] Mechanical Engineering Department, Faculty of Engineering, Kafrelsheikh University, Kafrelsheikh 33516, Egypt
[d] Nano Interface Center for Energy (NICE), School of Energy and Power Engineering, Huazhong University of Science and Technology, Wuhan 430074, China
[e] Innovation Institute Huazhong University of Science and Technology, Wuhan 430074, China
[f] Production Engineering and Mechanical Design Department, Faculty of Engineering, Tanta University, Tanta, Egypt
[g] Mechanical Engineering Department, Faculty of Engineering, University of Blue Nile, Al-Roseires, Blue Nile State, Sudan
[h] Department of Mechanical Engineering, Alsalama College of Sciences & Technology (ACST), Khartoum Bahri, Sudan
[i] Agricultural Engineering Department, Faculty of Agriculture, Kafrelsheikh University, 33516, Egypt
[j] Physics and Mathematical Engineering Department, Faculty of Electronic Engineering, Menoufiya University, Egypt
[k] Mechanical Power Engineering Department, Faculty of Engineering, Tanta University, Tanta, Egypt

ARTICLE INFO

Keywords:
Solar desalination
Energy
Exergy
Efficiency
Exergy destruction
Micro/nano particles

ABSTRACT

In this paper, a theoretical comparative study between modified solar stills (MSSs) and classical solar still (CSS) was carried out, based on the productivity and the thermal properties. The MSSs contain brackish water mixed with either graphite or copper oxide (CuO) micro/nano particles. Cost estimations of solar still desalination by using micro/nano particles was estimated. exergy destruction in various components of the solar still (SS) were calculated, analyzed and discussed. The exergy loss during the day time comprises the exergy destruction in the main components of the SS like basin plate, brine water, glazier plate and insulation material. The hourly convective, evaporative and radiative heat transfer coefficients (HTCs) with and without micro/nano particles were determined. The exergy destruction in various components of the SS have been analyzed and a solution was suggested. Results revealed that the exergy of evaporation, energy efficiency and exergy efficiency of MSSs were higher than that of the classical one. The daytime energy efficiencies of MSSs with graphite and CuO were 41.18% and 38.61%, respectively, but for the CSS was only 29.17%. The diurnal productivity of the MSSs was increased by 41.18% and 32.35% for graphite and CuO, respectively, compared with CSS. Moreover, the diurnal exergy efficiencies of MSSs were 4.32% and 3.78% for graphite and CuO respectively, while exergy efficiency for CSS was 2.63%. Furthermore, the costs of water production were found to be approximately 0.20, 0.21 and 0.24 RMB/L (1 RMB = 0.15 US $) when using MSS with CuO, MSS with graphite and CSS, respectively.

1. Introduction

Only 1% of obtainable water resources on the earth is drinkable, 2% is frozen in polar glaciers and the remnant of them about 97% are brackish and saline [1]. The commonly type used for solar desalination is the solar still (SS) due to its simplicity, low manufacturing cost, low operation and maintenance costs in addition, it doesn't need power source [2]. Exergy and energy analyses are used in assessing the performance of SSs, by monitoring the heat exchange (gaining or losing) process between the SS and its surroundings. Due to low yield of the SSs, many investigators introduced several scrupulous designs to enhance the output by enhancing the evaporation rate of water.

The developed designs include the double slope stepped SS with continual water circulation [3], stepped SS [4], SS with phase change materials (PCMs) [5], hybrid SS [6], SS with storage materials [7], SS with PV/T [8] and SS with vertical ripple surface [9]. Active single solar still (ASSS) and active double slope solar still (ADSSS) were integrated with N-thermal photovoltaic (PVT) and water parabolic collectors in order to optimize the number of collectors, water depth and mass flow rate. The analyses of enviroeconomic, productivity and

* Corresponding author at: State Key Laboratory of Coal Combustion, Huazhong University of Science and Technology, Wuhan 430074, China.
E-mail address: nuo@hust.edu.cn (N. Yang).

https://doi.org/10.1016/j.enconman.2018.09.074
Received 3 July 2018; Received in revised form 21 September 2018; Accepted 25 September 2018

Nomenclature

CSS	conventional solar still
MSSs	modified solar stills
SS with CuO = 1	solar still with copper oxid particle
SS with Graphite = 2	solar still with Graphite flakes
HTCs	heat transfer coefficients
ASSS	active single solar still
ADSSS	active double slope solar still
PVT	thermal photovoltaic
FPC	flat plate collector
GMF	graphite micro/nano-flakes
PDSSS	passive double slope solar still
ADSSS	active double slope solar still
I(t)	solar radiation, W/m^2
V_a	air speed, m/s
Cp	specific heat, kJ/kg K
T_a	air temperature, K
T_b	CSS basin temperature, K
T_w	CSS water temperature, K
T_{go}	CSS inlet glass temperature, K
T_{gi}	CSS outer glass temperature, K
T_{b1}	basin temperature of SS with CuO, K
T_{w1}	water temperature of SS with CuO, K
T_{go1}	inlet glass temperature of SS with CuO, K
T_{gi1}	outer glass temperature of SS with CuO, K
T_{b2}	basin temperature of SS with Graphite, K
T_{w2}	water temperature of SS with Graphite, K
T_{go2}	inlet glass temperature of SS with Graphite, K
T_{gi2}	outer glass temperature of SS with Graphite, K
K_{sw}	saline water thermal conductivity, W/m K
K_{nf}	nanofluids thermal conductivity, W/m K
K_p	nanoparticles thermal conductivity, W/m K

Greek

ρ_{sw}	saline water density, kg/m^3
ρ_p	nanoparticles density, kg/m^3
μ_{sw}	saline water dynamic viscosity, kg/m s
ρ_{nf}	nanofluids density, kg/m^3
μ_{nf}	nanofluids dynamic viscosity, kg/m s

Subscripts

a	ambient
b	plate basin
nf	nanofluids
g	glazier
w	saline water

exergoeconomic were conducted and results revealed that, the ADSSS/PVT had best performance compared with ASSS at 0.14 m water dept [10]. Joshia and Tiwari [11] analyzed monthly the performance of active SS combined with a heat exchanger and integrated with N- PVT and water flat plate collector (FPC). Results indicated that the FPC and PVT had high performance.

The major parameters influenced the yield of SS are the heat transfer mechanism and operating temperature. The coefficient of heat transfer can be improved by enhancing the thermal properties of the base water. Suspending nanoparticles into the base fluid is a very simple technique which enhances the thermal behavior and productivity. Nanofluid can be formed by suspending nano-sized particles in a base fluid. Using Al_2O_3, SnO_2 and ZnO nanofluids led to increase the SS yield by 29.95%, 18.63% and 12.67%, respectively compared without using nanofluids [12]. The integration of Al_2O_3 and CuO_2 nanoparticles and a condenser with a SS under the Egyptian conditions was investigated by Kabeel et al. [13]. Results revealed that the total diurnal yield of SS was enhanced by 88.97% and 125% in case of using only vacuum and Al_2O_3 nanoparticles with vacuum, respectively. While using CuO_2 nanoparticles, improved the yield by 133.6% and 93.8% in case of with and without vacuum. The productivity of the SS by using 0.12% wt of Al_2O_3 nanoparticles mixed with 80 kg and 35 kg mass of water was increased by 8.4% and 12.2%, respectively [14]. Sharshir et al. [15] experimentally investigated the influence of various weight concentrations of graphite micro/nano -flakes (GMF) and CuO particles; brine depths, and glass cover cooling flow rates on the performance of SS. The optimal daily efficiency of the SSs with GMF and CuO was 49% and 46%, respectively, compared with 30% for classical still.

Sahota et al. [16] Analytically studied the hybrid passive double slope solar still (PDSSS) and active double slope solar still (ADSSS) which integrated with N-thermal photovoltaic (PVT), helical heat exchanger and water FPC with three types of nanofluids (CuO, Al_2O_3 and TiO_2) mixed with 50 kg of water. The results indicated that the daily fresh water output from the hybrid unit with CuO, Al_2O_3 and TiO_2 nanofluids were 11.45 L, 11.27 L and 10.7 L respectively.

Energy and exergy analyses are represented by quantitative and qualitative analyses of energy established on the 1st and 2nd laws of thermodynamics, respectively. Exergy is a tremendous gadget used to classify and understand the reasons of the system inadequacies as well as determine the magnitude and location of these inefficiencies [17]. For all renewable energy systems, insufficient investigations were found in the literature on exergy analysis compared with energy analysis [17]. Dwivedi and Tiwari [18] used energy analysis to analyze the thermal performance of an active SS. It has been reported that the active SS productivity enhanced by 51% compared with passive one. Vaithilingam et al. [19] studied the exergy and energy efficiencies of a passive single slope SS as well as the exergy devastation of various SS components under different water depths. Ranjan et al. [20] conducted an exergy and energy analysis for SSs. They found that the exergy efficiency was smaller than the energy efficiency. The rate of exergy destruction in the SS components equal to 9.7, 62.5 and 386 W/m^2 for the glazier, water, and the bottom trough, respectively. Tiwari et al. [21] compared the passive and active SSs by analyzing their thermal performance via exergy and energy analyses. They pointed out that, the thermal efficiency was decreased by increasing the number of collectors and brine depth. The effect of using different nanofluids with different concentrations on the SS productivity has been investigated [22] However, for the best of knowledge, the SS thermal performance such as energy efficiency, exergy efficiency and exergy destruction with nanofluids has not been investigated.

The present study aims to show a theoretical investigation on the influence of micro/nano particles on solar still desalination. It includes: (i) the energy efficiency, exergy efficiency, cost estimation of SSs; (ii) the evaporative, radiative and convective heat transfer coefficients of SSs; (iii) the evaporation exergy and the production; (iv) the exergy efficiencies and destruction exergy of components, such as basin plate, glazier and brackish water.

2. Experimental setup and uncertainty analysis

Three similar SSs type L shape were designed, fabricated and used as the main components of the experimental setup. One SS was used as CSS without any modifications, while the other two stills were modified by adding graphite nanofluid to the first one and CuO nanofluid to the second one as illustrated in Fig. 1(a) and (b). The main body of SSs was made of welded iron sheets of 0.15 cm thick. Basin area for all stills was

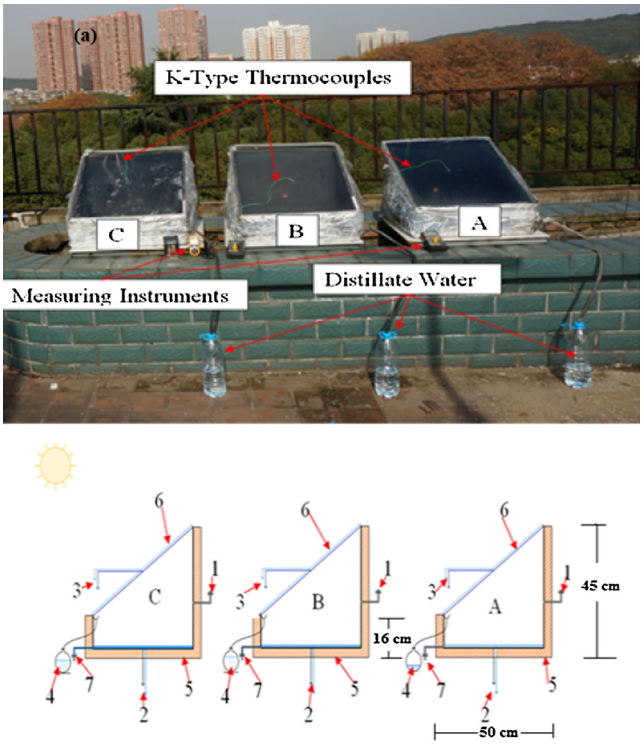

Fig. 1. (a) Picture of the experimental setup, (b) Schematic diagram of the experimental setup A: The CSS fed with water only, B: The MSS fed with water and CuO micro particles, C: The MSS fed with water and Graphite nanoparticles 1: Inlet fluid 2: Water and basin thermocouples 3: Inner and outer glazier thermocouples 4: Distilled water 5: Insulation (Fiber-glass) 6: Glass cover 7: Drain tap.

0.25 m^2 (0.5 m length × 0.5 m width). The height of low and high sides were 16 cm and 45 cm, respectively. The inner surfaces of the basin were coated by a black paint, which has a positive effect on harvesting solar energy and improving the evaporation rate. All external sides and bottoms of SSs were insulated by fiberglass to minimize heat losses to the ambient air. The upper surface of the basin was covered with glass sheet which inclined with 30° (almost the latitude angle of Wuhan, Hubei, China).

Experiments were carried out at the energy and power engineering school, Huazhong University of Science and Technology, Wuhan, China during October and November 2015. The experiments were conducted within daytime from 9 am to 5 pm. During the experiments, total solar intensity, the brine and glass temperatures, air speed, ambient temperature and the distillated water are measured at hourly interval.

The specifications of measuring instruments based on the commercial types used through the study, accuracy, range and computed experimental errors are tabulated in Table 1. The uncertainties in the obtained experimental results were calculated. The uncertainty limits of the temperature measurement were about 0.05 °C which calculated according to the following equation [23], considering the freezing and boiling temperatures for water (0 °C and 100 °C):

$$S_T = \left[\left(\frac{\partial T_a}{\partial T_{b,m}} S_{T_{b,m}} \right)^2 + \left(\frac{\partial T_a}{\partial T_{f,m}} S_{T_{f,m}} \right)^2 + \left(\frac{\partial T_a}{\partial T_m} S_{T_m} \right)^2 \right]^{1/2} \quad (1)$$

where T_a, $T_{b,m}$, $T_{f,m}$, and T_m are the actual, measured boiling, measured freezing and mean temperatures, respectively. And$S_{T_{b,m}}$, $S_{T_{f,m}}$, and $S_{T_m}$are the uncertainties in$T_{b,m}$, $T_{f,m}$, and T_m, respectively, and they have the same values for all thermocouples used in experiments.

3. Heat transfer analysis in solar stills

Depending on the transferred energy from or into the SS, the heat transfer process is classified as internal and external [24]. The internal heat transfer process is responsible for water heating and evaporation process as well as circulation of air inside the still. The nanofluid thermo-physical properties play an important role in this process. The external heat transfer is responsible for vapor condensation on the inner glass surface via heat exchange between the glass cover and surroundings.

The following assumptions have been assumed during our study:

1. Steady-state condition.
2. No vapor leakage occurs from the solar stills.
3. There are no temperature gradients across the water depth.
4. Heat losses is neglected.
5. No pumping, fuel, electricity as well as no chemical reactions

Both types of heat transfer processes, as well as, the thermo-physical properties of the nanofluids, are briefly discussed in the following sections.

3.1. Thermo-physical properties of water-nanoparticles mixture

Nanofluids have many superior properties compared with its traditional fluid like high absorptivity, high thermal conductivity, which may improve the productivity of the SSs [15]. Most physical properties of nanofluids can be described as functions of the base fluid and the nanoparticles properties. The equations of the main properties of nanofluids are given as:

nanofluids density [25]:

$$\rho_{nf} = \left(\frac{\varphi}{100} \right) \rho_p + \left(1 - \frac{\varphi}{100} \right) \rho_{sw} \quad (2)$$

where φ is the weight percentage and is given as:

$$\varphi = \left(\frac{m_p}{m_p + m_{sw}} \right) \times 100 \quad (3)$$

nanofluids specific heat [25]

$$C_{nf} = \frac{(\varphi/100)\rho_p C_p + (1-(\varphi/100))\rho_{sw} C_{sw}}{\rho_{nf}} \quad (4)$$

nanofluids thermal conductivity [26]

$$K_{nf} = K_{sw} \frac{K_p + (n-1)K_{sw} - (n-1)\varphi(K_{sw} - K_p)}{K_p + (n-1)K_{sw} + \varphi(K_{sw} - K_p)} \quad (5)$$

Inside the SS enclosure, the radiation and convection modes of heat

Table 1
Measuring instruments specifications.

Measured parameter	Instrument	Range	Accuracy	% Error
Temperature	Thermocouples of calibrated copper constantan type with a temperature indicator (digital model TES-1310)	−50 to 280 °C	± 1 °C	0.5
Solar intensity	Pyranometer (model TES-1333)	0–2000 W/m^2	± 10 W/m^2	0.25
Air velocity	Digital anemometer of vane type (Model Benetech GM816)	0–30 m/s	± 1 m/s	5
Productivity	Graded cylinder	1.5 L	± 0.002 L	10

transfer are occurred simultaneously. The heat energy is lost to the ambient air from the outer surface of the glazier by convection and radiation. The related heat transfer equations are mentioned as follow:

(i) Convection heat transfer (CHT)

The rate of the CHT occurs between the surface of water and the inner surface of the glass through water vapor due to the difference in temperature. Temperatures of water (T_w) and inner surface of the glass (T_{gi}) were used to point out the CHT rate into the still and is given by Velmurugan et al. [23].

$$Q_{C,w-gi} = h_{C,w-gi} \times (T_w - T_{gi}) \tag{6}$$

where $h_{C,w-gi}$ is the coefficient of CHT between the surface of water as well as the inner surface of the glass, as

$$h_{C,w-gi} = 0.884\left\{(T_w - T_{gi}) + \frac{[P_w - P_{gi}][T_w]}{[268900 - p_w]}\right\}^{1/3} \tag{7}$$

where P_w and P_{gi} are the partial pressure of water vapor at the surface of water and the glazier inner surface, respectively, which are given by Sharshir et al. [17]:

$$P_w = \exp\left[25.317 - \frac{5144}{T_w}\right] \tag{8}$$

$$P_{gi} = \exp\left[25.317 - \frac{5144}{T_{gi}}\right] \tag{9}$$

(ii) Radiation heat transfer (RHT)

The RHT rate between water and the glass internal surface which mentioned by Velmurugan et al. [23] is

$$Q_{R,w-gi} = h_{R,w-gi} \times (T_w - T_{gi}) \tag{10}$$

where $h_{R,w-gi}$ is the coefficient of RHT between water and the glass internal surface is

$$h_{R,w-gi} = \varepsilon_{eff}\sigma[(T_w)^2 + (T_{gi})^2](T_w + T_{gi}) \tag{11}$$

where ε_{eff} is the effective emissivity between the water and the glass internal surface which is expressed as:

$$\varepsilon_{eff} = \left(\frac{1}{\varepsilon_w} + \frac{1}{\varepsilon_g} - 1\right)^{-1} \tag{12}$$

(iii) Evaporative heat transfer (ETH)

The rate of the EHT occurs between water interface and water vapor. The EHT rate between saline water and glass internal surface is mentioned by Velmurugan et al. [23] as

$$Q_{E,w-gi} = h_{E,w-gi} \times (T_w - T_{gi}) \tag{13}$$

where $h_{E,w-gi}$ is the coefficient of EHT between water and the glass internal mentioned as

$$h_{E,w-gi} = 16.273 \times 10^{-3} \times h_{C,w-gi} \times \left[\frac{P_w - P_{gi}}{T_w - T_{gi}}\right] \tag{14}$$

The total coefficient of internal heat transfer between water mass and the glass internal surface ($h_{T,w-gi}$) is estimated using the following equation:

$$h_{T,w-gi} = h_{C,w-gi} + h_{R,w-gi} + h_{E,w-gi} \tag{15}$$

(iv) Top loss heat transfer

The top loss heat from external glazing surface is lost to ambient air by radiation and convection. The convection heat loss from glazing outer surface of still to the ambient is given by Velmurugan et al. [23] as

$$Q_{C,go-a} = h_{C,go-a}A_g(T_{go} - T_a) \tag{16}$$

where the CHT coefficient ($h_{C,go-a}$) is presented as a function of air speed (v) as:

$$h_{C,go-a} = 2.8 + (3.0 \times v) \tag{17}$$

The rate of radiation heat loss from glass outer surface and the ambient is evaluated as:

$$Q_{R,go-a} = h_{R,go-a}A_w(T_{go} - T_a) \tag{18}$$

The RHT coefficient ($h_{R,go-a}$) between glass external surface and the atmosphere is obtained as:

$$h_{R,go-a} = \varepsilon_g\sigma\left[\frac{(T_{go})^4 - (T_{Sky})^4}{(T_{go} - T_a)}\right] \tag{19}$$

where

$$T_{Sky} = 0.0552 \times T_a^{1.5} \tag{20}$$

The total rate of top heat loss is the collection of convective and radiative losses which is estimated from:

$$Q_{T,go-a} = h_{T,go-a}A_g(T_{go} - T_a) \tag{21}$$

The total coefficient of top loss between outer glass surface and the ambient air is calculated by the following:

$$h_{T,go-a} = h_{C,go-a} + h_{R,go-a} \tag{22}$$

Or, it can be estimated as a function of air speed (v) as:

$$h_{T,go-a} = 5.7 + (3.8 \times v) \tag{23}$$

The rate of heat gained from the feed water $Q_{mw}$is calculated by the following:

$$Q_{mw} = m_{SS}(T_a - T_w) \tag{24}$$

(v) Loss heat transfer from basin bottom and sides

The rate of CHT between water and the basin is obtained by the following equation [27]

$$Q_w = h_w A_b(T_b - T_w) \tag{25}$$

where h_w is the coefficient of CHT from water to the basin as:

$$h_w = 0.54\frac{K_w}{L}(Gr\,\mathrm{Pr})^{0.25} \tag{26}$$

where the CHT rate between the basin and ambient air is given as:

$$Q_b = h_b A_b(T_b - T_a) \tag{27}$$

The coefficient of heat transfer between surrounding air and the basin through the insulation is given as:

$$h_b = \left[\frac{L_{ins}}{K_{ins}} + \frac{1}{h_{T,b-a}}\right]^{-1} \tag{28}$$

where,

$$h_{T,b-a} = 5.7 + (3.8 \times v) \tag{29}$$

Above sections described the analysis of heat transfer from or into the solar still, now the following equations describe the energy balance through the still components such as basin, water and glass as pointed out by Velmurugan et al. [23].

Energy balance of the basin is given as:

$$m_b c_{pb}(dT_b/dt) = I(t)A_b\alpha_b - Q_w - Q_b \tag{30}$$

Energy balance of water is given as:

$$m_w c_{pw}(dT_w/dt) = I(t)A_w\alpha_w + Q_w - Q_{Cw-gi} - Q_{R,w-gi} - Q_{E,w-gi} - Q_{mw} \quad (31)$$

Energy balance for the still with nano/micro particles is given as:

$$m_{nf} c_{pnf}(dT_{nf}/dt) = I(t)A_w\alpha_{nf} + Q_w - Q_{Cw-gi} - Q_{R,w-gi} - Q_{E,w-gi} - Q_{mw} \quad (32)$$

Energy balance of the glass cover is given as:

$$m_g c_{pg}(dT_g/dt) = I(t)A_g\alpha_g + Q_{Cw-gi} + Q_{R,w-gi} + Q_{E,w-gi} - Q_{R,go-a} - Q_{C,go-a} \quad (33)$$

Productivity of the still can be obtained as:

$$m_{SS} = \frac{Q_{E,w-gi}}{h_{fg}} \quad (34)$$

3.2. Thermal efficiency of solar still based on energy/exergy analysis

Energy efficiency plays an important role in assessing SSs performance [21]. The total efficiency, η, is defined as the accumulated yield $\sum m_{ew}$ (kg) multiplied by the latent heat of evaporation h_{fg} (J/kg) divided by the summation of insolation $I(t)$ over the glass cover area A_s, and is given by:

$$\eta = \frac{\sum m_{ew} \times h_{fg}}{\sum I(t) \times A_s \times 3600} \quad (35)$$

Detailed information regarding exergy balance equations for the three essential components of the SS (basin water, basin-liner, and glazier) can be found in [17]. Assuming that the thermal capacity of SS components is negligible, thus the accumulation of exergy is neglected. The investigation of exergy-based on the 2nd law of thermodynamics is used to represent the energy quality by identifying and understanding the causes of the system inefficiencies. Moreover, it is used to determine the magnitude and locations of these inefficiencies. The exergy efficiency of SS (η_{EX}) is given as the ratio between the exergy output and input of the SS, i.e., distillate water exergy to the insolation exergy [21].

$$\eta_{EX} = \frac{\text{Exergy output of solar still}}{\text{Exergy input of solar still}} = \frac{E_{x_{evap}}}{E_{x_{input}}} \quad (36)$$

In the SS, the output exergy is related to evaporation and condensation of water. However, as some of the condensate water on the inner surface of the glass cover falls back into the basin, the exergy output based on the experimental results differs from the theoretical one. The hourly exergy output of SS is calculated from the following equation [21].

$$E_{x_{output}} = E_{x_{evap}} = \frac{\dot{m_{ew}} \times h_{fg}}{(3600\,\text{s h}^{-1})} \times \left(1 - \frac{T_a}{T_w}\right) \quad (37)$$

where $T_a$is the ambient temperature (°C) and T_w is the water temperature (°C).

The exergy input to SS ($E_{x_{sun}}$) represents the exergy of insolation and is given as [21].

$$E_{x_{sun}} = A_s \times I(t)_s \left[1 - \frac{4}{3} \times \left(\frac{T_a}{T_s}\right) + \frac{1}{3} \times \left(\frac{T_a}{T_s}\right)^4\right] \quad (38)$$

where $T_s$is the sun temperature (6000 K).

- Exergy balance equations

The equilibrium exergy equations for the still components (basin, water and glass) are analyzed. On the assumption that the thermal ability of the components is negligible, thus exergy accumulation is neglected. Furthermore, it is known that, the exergy loss and exergy destruction are two different concepts. Firstly, exergy loss (external phenomenon between system components and surrounding) represents the exergy content which is completely dissipated into the surroundings. In our work, the exergy can be lost from both the plate to the insulation and the glass to the ambient. Secondly, exergy destruction (internal phenomenon within system components) refers to the exergy that is destroyed due to irreversibility within system components. In our work, the exergy destruction occurs in glass, plate and water. The streams of exergy are illustrated in Fig. 2. Green, red and black arrows refer to useful exergy, exergy loss and exergy destruction, respectively)

- Absorber plate

Fig. 2(a) illustrates the exergy balance of the basin plate. From the figure, it can be observed that the basin plate absorbs part of solar exergy E_{Xsun} that reaches to its surface. This exergy is divided into three parts: The first part is beneficial exergy E_{Xw} which is used to heat the water in the base, the second part is a little that lost across the insulation E_{Xinsul}, while the remaining part is destroyed by the plate $E_{Xd,b}$ [27]:

$$E_{X_{d,b}} = (\alpha_b \times \tau_w \times \tau_g)E_{Xsun} - (E_{Xw} + E_{Xinsul}) \quad (39)$$

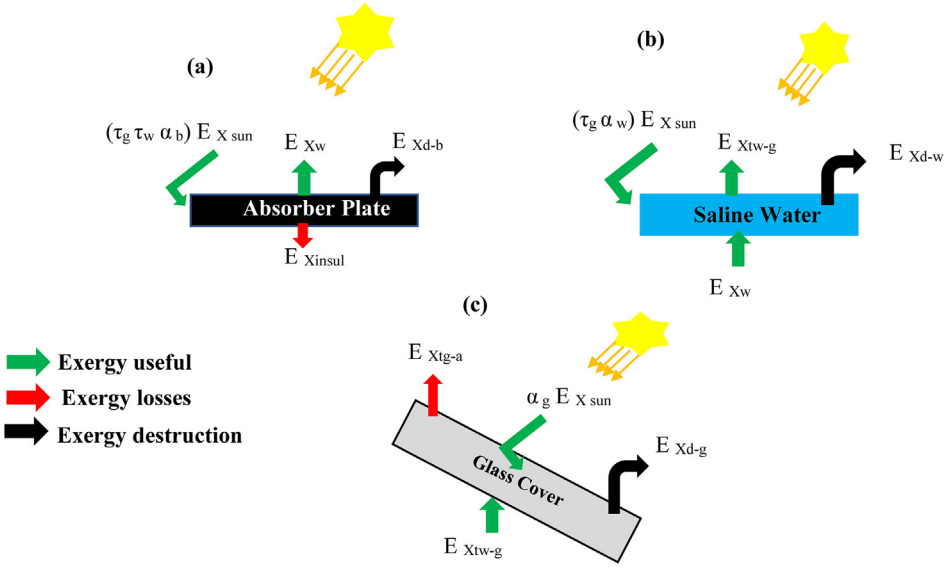

Fig. 2. Balance of exergy for (a) Absorber plate, (b) saline water and (c) glazier cover.

where

$$E_{X_W} = h_w(T_b - T_w)\left(1 - \frac{T_a}{T_b}\right) \quad (40)$$

and

$$E_{Xinsul} = h_b(T_b - T_a)\left(1 - \frac{T_a}{T_b}\right) \quad (41)$$

where α_b is the absorptivity of the plate, τ_w is the water transmittance andτ_g is the glass cover transmittance. The solar exergy per unit area E_{Xsun}, on the glazier is given as

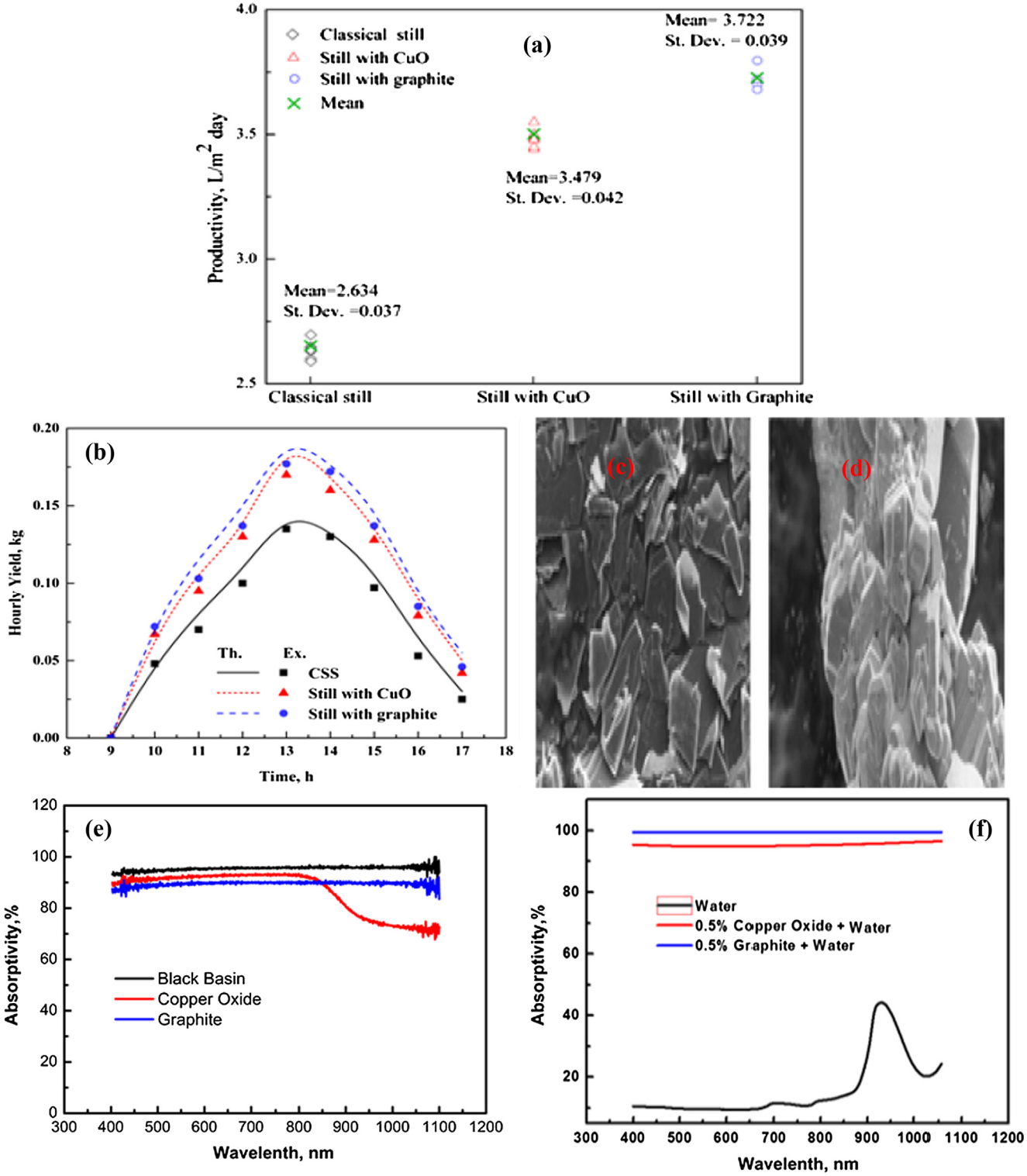

Fig. 3. (a) Productivity of six days and standard deviation as well as the mean productivity during these days. (b) Validation of the mathematical model with the experimental results of the three SSs. (c) SEM images of graphite micro/nano-flakes, (d) SEM images of copper oxide micro particles. (e) The absorption of the black paint, graphite micro/nano -flakes and copper oxide particles. (f) The absorption of water, mixtures of 0.5% uniform graphite and 0.5% copper oxide with water.

$$E_{Xsun} = I(t) \times \psi \tag{42}$$

where ψ is petela and $I(t)$is the insolation

$$\psi = \left[1 + \frac{1}{3}\left(\frac{T_a}{T_s}\right)^4 - \frac{4}{3}\left(\frac{T_a}{T_s}\right)\right] \tag{43}$$

- Saline water

Fig. 2(b) illustrates the exergy of the basin water (the input exergy to the saline water in the basin) [27]. The figure indicates that, solar exergy $(\tau_g \times \alpha_w)E_{Xsun}$, the useful exergy which come from the basin plate E_{Xw}, the exergy related to the heat transfer between the glazier cover and saline water into the still $E_{Xt,w-g}$, and the remaining part destroyed by the water$E_{Xd,w}$

$$E_{Xd,w} = (\tau_g \times \alpha_w) \times E_{Xsun} + E_{Xw} - E_{Xt,w-g} \tag{44}$$

where $\alpha_w$is the water absorptivity and $E_{Xt,w-g}$ is the result of total exergy which include the three parts as

$$E_{Xt,w-g} = E_{Xe,w-g} + E_{Xr,w-g} + E_{Xc,w-g} \tag{45}$$

where $E_{Xe,wg}$ evaporation exergy is given as

$$E_{Xe,w-g} = h_{e,w-g}(T_w - T_{gi})\left(1 - \frac{T_a}{T_w}\right) \tag{46}$$

and $E_{Xr,wg}$ radiation exergy is given as

$$E_{Xr,w-g} = h_{c,w-g}(T_w - T_{gi})\left(1 - \frac{T_a}{T_w}\right) \tag{47}$$

and $E_{Xc,wg}$ convection exergy is given as

$$E_{Xc,w-g} = h_{r,w-g}(T_w - T_{gi})\psi \tag{48}$$

- Glazier cover

Fig. 2(c) illustrates the exergy balance of glass cover [27]

$$E_{Xd,g} = \alpha_g \times E_{Xsun} + E_{Xt,wg} - E_{Xt,ga} \tag{49}$$

where α_g is the glazier absorptivity, $E_{Xt,g}$is the loss of exergy come from glazier heat losses to the ambient air due to the solar intensity $E_{Xr,ga}$, and convection exergy $E_{Xc,ga}$ is calculated by the following:

$$E_{Xt,ga} = E_{Xr,g-a} + E_{Xc,g-a} \tag{50}$$

where

$$E_{Xr,g-a} = h_{R,g-a} \times (T_{go} - T_a)\psi \tag{51}$$

$$E_{Xc,ga} = h_{C,ga}(T_{go} - T_a) \times \left(1 - \frac{T_a}{T_{go}}\right) \tag{52}$$

4. Results and discussion

Experiments were carried out during daytime and repeated six times for the three types of SSs within two months as shown in Fig. 3(a). ANOVA analysis was carried out to identify the variance in the obtained results. Fig. 3(a) illustrates productivity of six days as well as the mean productivity of those days. The mean values of the productivity for the CSS, still with CuO and still with graphite were 2.634, 3.479 and 3.722, respectively, while the standard deviation for the same three types of SSs were 0.037, 0.042 and 0.039, respectively. These results revealed the consistency for different days of experiments. Therefore, the data of 20th October was used in the analysis, where it had residuals of 0.002, −0.005, and 0.006 over the mean values of the productivity for the CSS, still with CuO and still with graphite, respectively.

4.1. Model validation

The mathematical model based on the energy equations for CSS, still with CuO and still with graphite was verified using experimental data. Fig. 3(b) illustrates the comparison between the mathematical model and experimental results for the three stills. It is clear that there was a good agreement between the mathematical model and experimental results. The divergence between theoretical and experimental data were about 7%, 6.6, 6.5% for the CSS, still with CuO and still with graphite, respectively. This divergence may be due to the surrounding conditions which are considered constant with time, in the mathematical solution, while they varying with time in the experimental work.

4.2. Materials and nanofluids characterization

The morphology of the graphite micro/nano -flakes and the copper oxide particles were measured by scanning electron microscope (Helios Nanolab G3 CX) and illustrated in Fig. 3(c) and (d). It is obvious that the graphite particles have large lateral size and small thickness, hence it has a flake shape. The graphite micro/nano -flakes particles are 10,000 meshes and they are procured from the local market. The lateral flakes size was about 1.3 μm and 100 nm thickness as shown in Fig. 3(c). The morphology of CuO particles is cuboid, where their size is about 1 μm. Unlike graphite particles, the copper oxide particles aggregated tightly, where the size of the aggregated particles is about 1 μm as shown in Fig. 3(d). The specifications of graphite and CuO particles are presented in Table 2.

Compared with the absorbing plate surface, the absorptivity of the 3D absorbing materials like porous material and nanofluid is high due to the multiple scattering and absorption of the light. The absorption characteristics of the materials used in this study were measured by UV–Vis (LabRAM HR800) at 400–1100 nm wavelength as shown in Fig. 3(e) and (f) compared with the absorption of the black basin of 94%. The absorption of the uniform graphite micro/nano -flakes is around 90% which is lower than that of the black paint by 4%. Whereas the absorption of copper oxide particles is around 91.5%, which is lower than that of the black paint by about 2.5% and higher than that of the graphite micro/nano-flakes by about 1.5%. This absorption is given until 850 nm wavelength after that, from 850 to 1200 nm the copper oxide particles decrease to about 70% as shown in Fig. 3(e). Furthermore, Fig. 3(f). illustrates the absorption of pure water, 0.5% graphite nanofluids and 0.5 copper oxide nanofluids. From Fig. 3(f) the absorption of the 0.5% uniform graphite nanofluid is around 99.5%, which is higher than that of the black paint (~94%) by 5.5% and higher than that of graphite micro/nano-flakes by about 9.5%. This is because of the 3D absorbing structure of the graphite nanofluid, in which light is trapped on the graphite flakes surface and subjected to multiple absorption.

On the other hand, the absorption of 0.5% copper oxide nanofluid is around 96%, which is higher than that of both black paint and copper oxide particles by 2% and 4.5%, respectively. This is due to light trapping in case of graphite flakes as discussed above.

The thermophysical properties of nanofluids such as thermal conductivity, density and absorption are much higher than that of the base fluid due to the effect of nanoparticles [22,25]. The nanoparticles have high ratio of surface area to volume, which enhances their absorption of the insolation. The high density of nanofluids coupled with the low

Table 2
Specifications of nanoparticles.

Specifications	Graphite	CuO
Thermal conductivity, W/(m K)	129.0	76.0
Density, g/cm^3	1.20	6.40
Average particles size	1.2 μm ×100 nm	~1 μm

specific heat of nanoparticles results in enhancing their onvection HTC. Increasing the nanofluid thermal conductivity led to increase the HTCs which in turn increased the amount of evaporation and consequently the productivity.

4.3. Effect of meteorological parameters on the solar stills performance

The effect of hourly insolation, air velocity and air temperature on the thermal performance of SSs (CSS, SS with CuO, SS with Graphite) for one day of experiments is given in Table 3. Effect of CuO and graphite nanofluids on the performance of still at 0.5 cm water depth and 1% concentration is discussed. As shown in table, and as expected, all temperatures of brine water, plate and glazier are raised gradually with the raise of insolation and reached peak values at approximately hour 13, thereafter the insolation and ingredients temperatures are depressed. In addition, the brine water, basin plate, inner glass surface, and outer glass surface temperatures in case of SS with graphite nanofluid were more than that of the CSS by 1.5–4.5 °C, 0.9–4 °C, 0.2–3.5 °C, and 0.5–2 °C, respectively. While, the basin plate, brine water, inner glass surface, and outer glass surface temperatures in case of SS with CuO nanofluid were higher than that of the CSS by 1.2–4 °C, 1.6–4.1 °C, 0.5–3 °C, and 0.5–2 °C, respectively. Due to this temperature difference, water evaporation and productivity of MSSs were higher than that of CSS.

4.4. Hourly convective, evaporative and radiative heat transfer coefficients with/without micro/nano particles

The hourly convective, evaporative and radiative heat transfer coefficients (HTCs) of CSS and MSSs with graphite and copper oxide particles at a weight concentration of 1% and 0.5 cm water depth are shown in Fig. 4. The convective and evaporative HTCs have significant values for MSSs with graphite and CuO particles compared with CSS. Convective HTC of CSS ranged from 1.20 to 2.39 W/m^2 K, while MSS with CuO and graphite ranged from 1.42 to 2.58 W/m^2 K and from 1.42 to 2.65 W/m^2 K, respectively as illustrated in Fig. 4(a). These results may be due to the higher temperature in MSSs compared with CSS. Furthermore, the evaporative HTC values of MSSs changed from 8 to 58 W/m^2 K for graphite nanoparticles and from 8 to 56 W/m^2 K for CuO microparticles, while for CSS it varied from 8 to 47 W/m^2 K, as shown in Fig. 4(b). The higher evaporative HTC in MSSs was also recorded due to the higher temperature in MSSs compared with CSS.

Fig. 4(c) shows the hourly rate of radiative HTC between the water and glazier. The radiative HTC between the water and glazier in MSSs was little higher than CSS because the temperature differences between the basin water and the inner surfaces of the glass cover which were high in MSSs compared with CSS.

4.5. Exergy of evaporation and fresh water productivity

Basin water was heated up and began to evaporate under the effect of an evaporative heat flux. The exergy of evaporation for the MSSs as well as CSS are shown in Fig. 5(a). The exergy of evaporation was increased to its peak at hour 13 for all SSs with and without nanofluids. These values were 14.33, 13.70 and 10.23 W for the graphite nanofluid, copper oxide nanofluid and CSS, respectively. For modified stills with nanoparticles (graphite and copper oxide) the water temperature was higher than the CSS. As a result, evaporation rate and the exergy of evaporation were high in case of SSs provided with graphite and CuO nanofluids. Therefore, the productivity of the nanofluids stills was higher than that of the CSS.

The variations of hourly productivity for MSSs and CSS are plotted in Fig. 5(b). It can be noticed from Fig. 5(b) that the productivity followed similar trend of the evaporation exergy as observed from Fig. 5(a). The output of modified stills increased compared with the CSS because there was a significant increase in the evaporation rate, as a result of increasing the heat transfer rate due to using the nanofluids. The diurnal productivity of MSSs with the graphite and CuO nanofluid were enhanced by 41.18% and 32.35%, respectively, compared with CSS.

4.6. Exergy destruction and exergy efficiency in still components

The quantity and location of exergy destruction could be identified through exergy analysis. Therefore, the exergy efficiency would by reducing the exergy destruction in various SS components via applying suitable measures and modifications. The instantaneous exergy destruction rate for different SS components (saline water, basin liner, and glazing cover) was calculated.

Variation of exergy destruction in basin plate based on hourly intervals is illustrated in Fig. 6(a). The highest daily exergy destruction of 12384 kJ/m^2 day in basin liner with and without nanofluids was almost the same at 0.5 cm water depth and 1% concentration of nanofluids. Moreover, as shown in that figure the exergy destruction of basin liner of SS with nanofluids was a bit little larger than that of CSS due to the lowest difference in temperature ($T_b - T_w$) between basin plate and the brackish water in MSSs compared with CSS. The exergy destruction values in the present study are in agreement with Zoori et al. [27]. The highest exergy destruction was observed in the basin plate. This may refer to lower temperature difference between basin plate and the brackish water.

Fig. 6(a) shows the exergy destruction that occurs in the glazing cover. It was found that, the glazing cover exergy destruction in modified SSs was higher than that of CSS. This may be due to higher difference in temperature between the glazing cover and ambient air for the MSSs compared to the CSS. The maximum daily exergy destruction of the glazing cover occurs in the still with graphite nanofluid, CuO nanofluid and CSS were 1492, 1419 and 911 kJ/m^2 day.

The lowest exergy destruction was obtained in the saline water as shown in Fig. 6(a). It was noticed that the exergy destruction in the saline water was decreased by enhancing the difference in temperature between saline water and the internal glass surface ($T_w - T_{gi}$). This

Table 3
Effect of meteorological parameters on the thermal behavior of SSs on October 20th, 2015.

Time	Meteorological parameters			CSS				SS with CuO				SS with Graphite			
	I(t) (W/m^2)	T_a (K)	V_a (m/s)	T_b (K)	T_w (K)	T_{go} (K)	T_{gi} (K)	T_{b1} (K)	T_{w1} (K)	T_{go1} (K)	T_{gi1} (K)	T_{b2} (K)	T_{w2} (K)	T_{go2} (K)	Tgi2 (K)
9	440	299	2.1	316.7	313.5	309	310.5	319	315.6	310	311	318	315.35	311	310.3
10	650	301	2	332.4	328.5	321	323.5	336.4	332.6	323	325.5	336.4	332.75	323	325.2
11	775	302	1.9	342.9	338.5	330	332.5	346.5	341.6	331	333.5	345.5	340.85	331.8	332.5
12	900	303	2.2	347.2	342.5	332	336.5	351	345.6	334	337.5	351	345.85	334	337.6
13	880	304	2.6	349.1	344.5	334	337.5	352.5	347.6	335	339.5	352.5	347.85	335.5	339.4
14	820	303	1.7	343.7	339.5	330.5	332.5	346	341.6	331	333.5	345	341	331.5	332.5
15	695	303	1	332	329.5	321	324.5	335.5	333.1	322	327.5	336	334	323	328
16	440	302	0.7	324.3	322	315	318	325.5	323.6	315.5	319	326	324.45	316.5	319.5
17	252	301	1.1	317.6	315.5	311	313.5	319.5	317.6	311.5	314.5	318.5	317.1	311.5	314

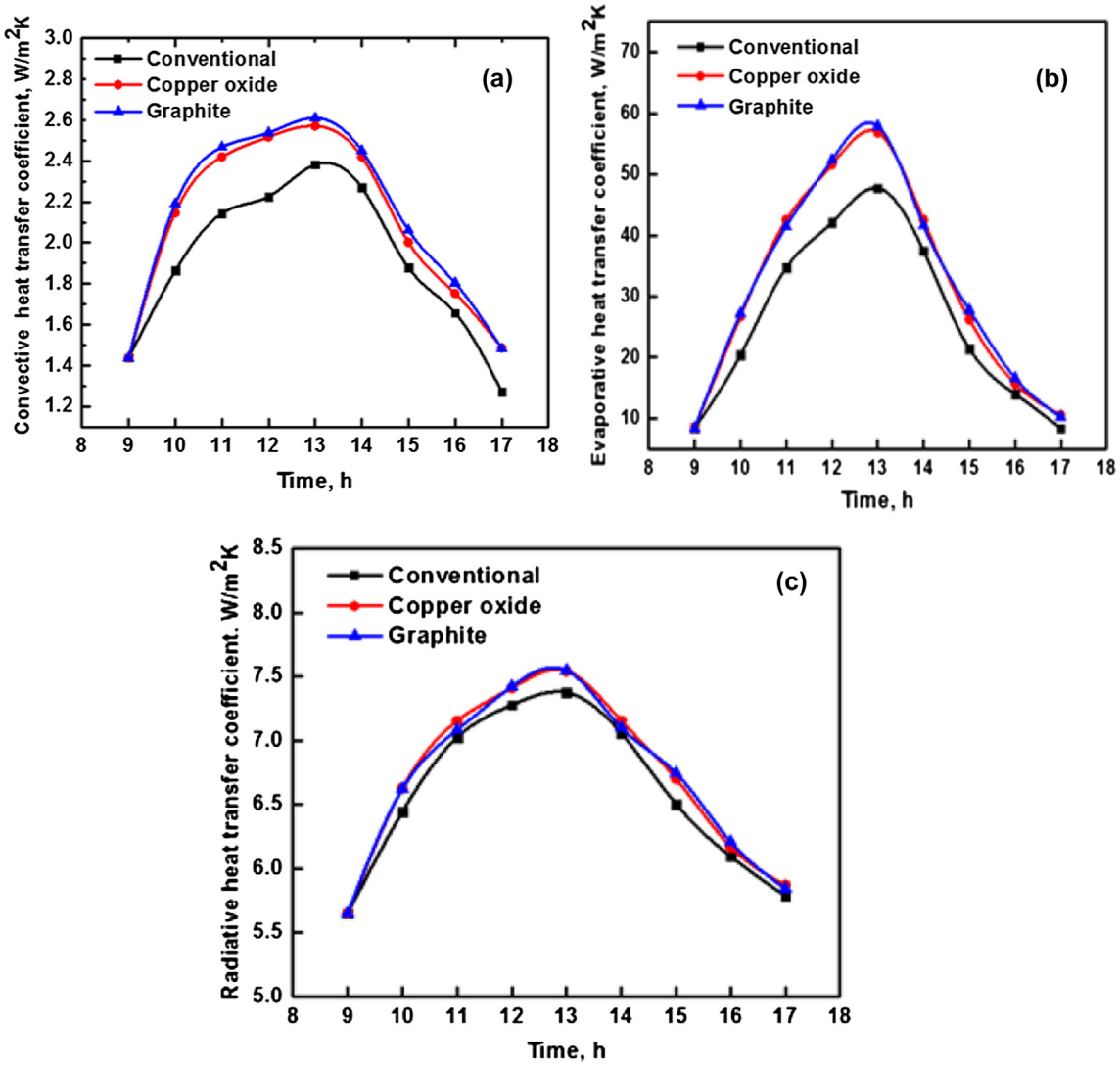

Fig. 4. Heat transfer coefficients (HTC) between water and glaizer of CSS and MSSs which occurred by convection (a), evaporation (b) and radiation (c).

increase in the temperature difference increased the exergy of evaporation (E_{xtw_g}) from the surface of water and decreased the exergy destruction of water. This in agreement with Vaithilingam and Esakkimuthu [19]. Hence, the exergy destruction of saline water with nanofluid was lower than that of the still without nanofluid due to the higher difference in temperature in the former compared with the latter case. Therefore, the evaporation rate in the MSSs was larger than that of CSS.

The high difference in temperature between plate surface and water leads to increase the exergy related to water (E_{xw}) and decrease the exergy destruction in the plate surface. The maximum diurnal exergy destruction of the water in the basin occurs in the modified SSs with nanofluids of graphite, copper oxide and CSS were 473, 787 and 1075 kJ/m^2 day, respectively.

Furthermore, Fig. 6(a) shows the exergy loss through insulation $E_{X_{ins}}$ for the MSSs and CSS. The daily insulation exergy loss in the MSSs with CuO and graphite were 1693.872 kJ/m^2 day and 1664.48 kJ/m^2 day, respectively, which were higher than that of the classical one (1447.128 kJ/m^2 day) by 17% for CuO and 15% for graphite. The reason for that refer to the large difference in temperature between the basin plate and the ambient in the MSSs compared to CSS. These high losses have high impact on the SS thermal performance. Therefore, care must be taken during the design process of SS, especially in the MSSs, to reduce the thermal energy losses by using prober insulations with lower thermal conductivity.

The diurnal exergy efficiencies of the CSS components, i.e., the basin liner, the glazing cover and the saline water, were 11.89%, 17.66% and 63.61%, respectively; these values were increased for the still with CuO nanofluid and reached about 13.40%, 23.18% and 80.83% for the same components, respectively. Moreover, these values were increased for the still with graphite nanofluid and reached about 12.32%, 23.76% and 93.35% for the same components (basin liner, glazing, and saline water), respectively, as shown in Fig. 6(b). Results depicted in Fig. 6(b) show a perfect agreement with basic laws of thermodynamics that the higher exergy destruction results in decreasing the energy and exergy efficiencies of SSs. These results may be beneficial for the further SSs design improvements to increase their productivity and obtain cost-effective efficiencies.

4.7. Diurnal energy and exergy efficiencies

The hourly energy efficiency is plotted in Fig. 7(a), where it begins to increase at the starting of the experiment and reached the peak value at approximately hour 14 for SSs understudy. The maximum hourly energy efficiency was 46.98% and 43.68% with graphite and CuO nanofluids, respectively, while it was 35.56% for the CSS (without nanofluid). Furthermore, the hourly exergy efficiency is illustrated in Fig. 7(b). Moreover, the hourly exergy efficiency begins to increase at

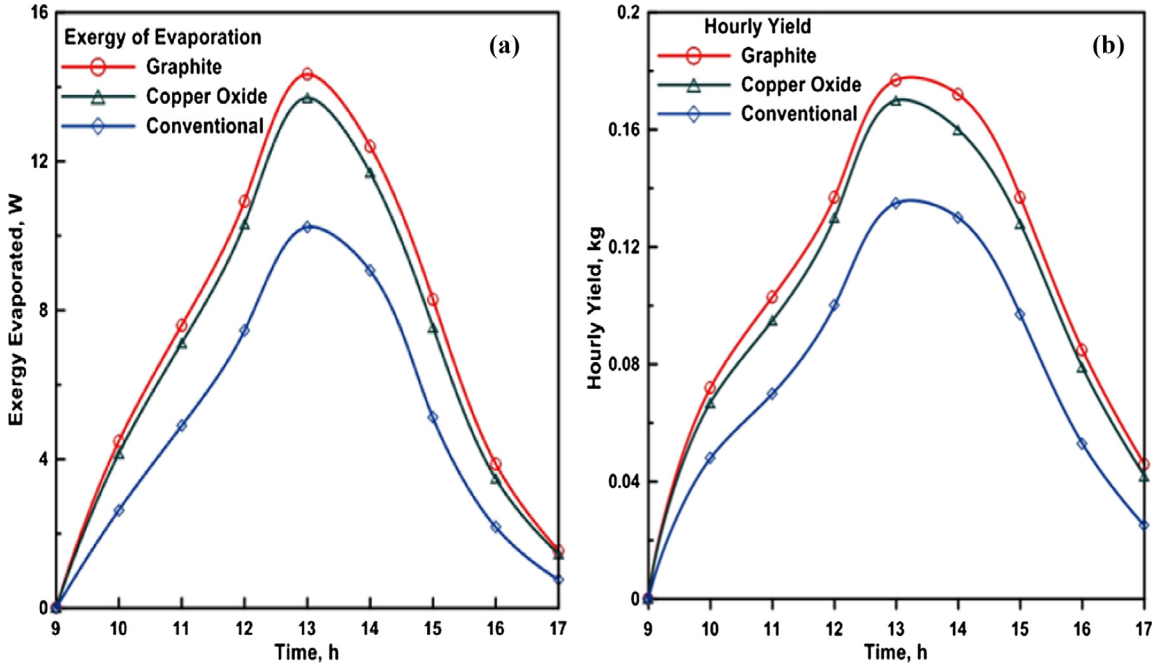

Fig. 5. Hourly variation of exergy of evaporation (a) and freshwater productivity (b) for SSs with and without nanofluids.

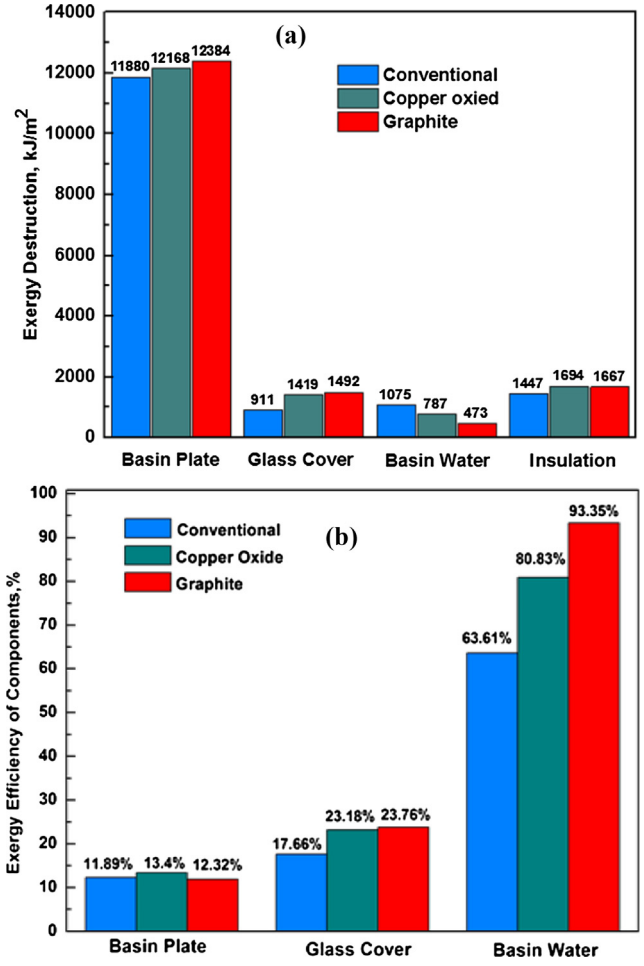

Fig. 6. (a) Diurnal variation of exergy destruction (a) and exergy efficiencies (b) for different SS components with different parameters.

the starting of the experiment and reached the peak value at approximately hour 13 for all SSs under investigation. This is because of the heat energy stored inside the saline water during the larger insolation time (from hour 9:0 to hour 13:0). The peak value of hourly exergy efficiency was 6.06% and 5.79% with graphite and CuO nanofluids, respectively, while it was 4.32% for the CSS. Furthermore, it was noticed that the energy efficiency was larger than the exergy efficiency for all SSs. The low value of exergy efficiency results from low quality or amount of evaporative thermal energy.

The daytime total exergy and energy efficiency for the MSSs and CSS are illustrated in Fig. 7(c). The diurnal energy efficiencies according to Eq. (35) for modified stills with graphite nanofluid, CuO nanofluid and CSS were 41.18%, 38.61%, and 29.17%, respectively. Furthermore, the diurnal exergy efficiencies according to Eq. (36) for modified stills with graphite nanofluid, CuO nanofluid, and CSS were 4.32%, 3.78% and 2.63%, respectively. So, it is recommended to use nanofluids in the stills, as they enhance the total thermal performance.

Table 4 presents a comparison between current work and previous works that used CuO nanoparticles to enhance the SSs productivity.

5. Cost estimation

For classical solar still (CSS), the overall constant price (CP) was 453 RMB (1$ US = 6.67 RMB-Chinese currency) according to the Chinese local market as shown in Table 5. For obtaining the average cost of water productivity, the overall price (OP) should be the summation of constant price and variable price (VP) as, OP = CP + VP. Considering that VP per year equals 30% of CP according to Omara et al. [31] and the life spans about 10 years, the value of OP was calculated as, OP = 453 + 0.30 × 453 × 10 = 1812 RMB. The average water production per day from the CSS was about 2.50 L/m^2 day. Assuming that, the CSS is working about 300 day/year, the overall fresh water production of CSS through the life was estimated as 7500 L. Then, the cost of one liter of fresh water from CSS was 0.24 RMB.

Based on the same calculation method, for MSS using copper oxide, the overall price was 2052 RMB. Furthermore, the total fresh water production through the life of still with copper oxide was 10,200 L. So, the cost of one litter fresh water equals 0.20 RMB where the average fresh water production was 3.40 L/m^2 day. Whereas, in case of using

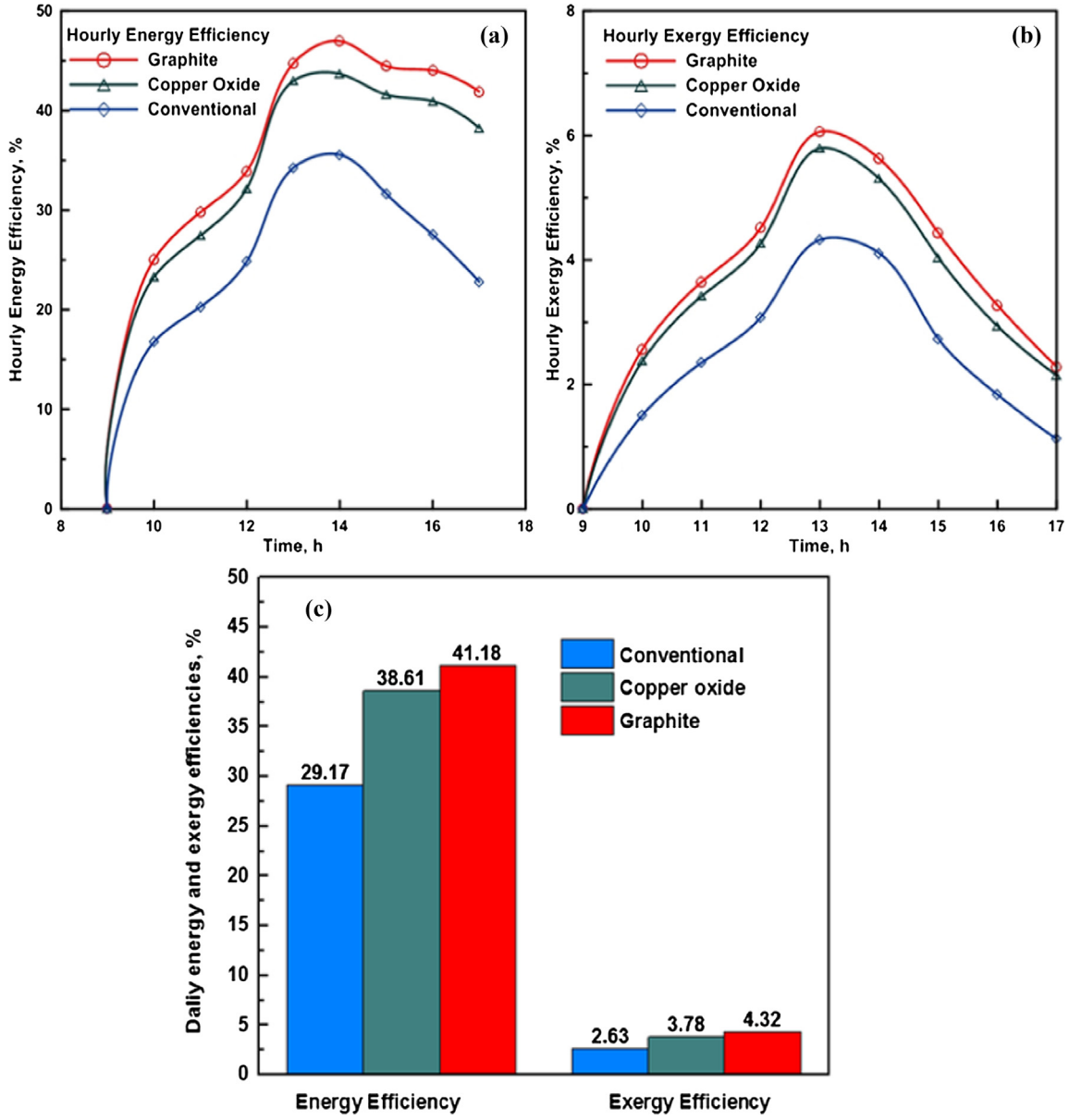

Fig. 7. Hourly variation of energy efficiency (a), exergy efficiency, (b) and diurnal exergy and energy efficiencies (c).

graphite nanoparticles in MSS, the overall price was 2292 RMB. The average fresh water production was 3.60 L/m^2 day. The total fresh water produced through the life of still using graphite was 10,800 L. The cost of one litter fresh water when using graphite was 0.21 RMB.

6. Conclusions

This study was conducted to figure out the influence of utilizing nanoparticles such as graphite and copper oxide on the thermal performance of SSs compared with a CSS (without nanofluids) at the same operating conditions. Firstly, the hourly, diurnal; and the total energy and exergy efficiencies are offered. The diurnal exergy efficiency is much inferior than the diurnal energy efficiency for MSSs as well as CSS. Moreover, the energy and exergy efficiencies are higher in case of MSSs compared with CSS. Secondly, the exergy destruction for all components of the stills understudy (basin, glazing, and water) are analyzed. It can be concluded that among all SS components, the basin has the largest exergy destruction, which may be decreased by selecting suitable materials for the basin liner and the insulation which result in enhancing the exergy efficiency of SSs. The outcomes can be summarized as follow:

- The diurnal exergy efficiency of graphite, CuO nanofluids and CSS were 4.32%, 3.78%, and 2.63%, respectively.
- The diurnal exergy efficiencies of the CSS components, i.e., basin, glazier and water, were 11.89%, 17.66% and 63.61%, respectively.
- The diurnal exergy efficiencies for components of the still with CuO nanofluid, i.e., basin, glazing cover and saline water were 13.40%, 23.18% and 80.83%, respectively.
- The diurnal exergy efficiencies for components of the still with graphite nanofluid, i.e., basin liner, glazing cover and saline water were 32%, 23.76% and 93.35%, respectively.
- The output of the stills with graphite and CuO nanofluid reached approximately 41.18% and 32.35%, respectively, over the classical one.
- The diurnal energy efficiencies for the still with graphite and CuO nanofluids were 41.18% and 38.61%, respectively, while for CSS it was 29.17%.
- The costs of water production were found to be approximately 0.20, 0.21 and 0.24 RMB/L when using MSS with CuO, MSS with graphite

Table 4
Comparison between current work and previous works that used CuO nanoparticles to enhance the SSs productivity.

Authors/References and Types of SSs	Locations and (Latitude)	Types and size of particles	Nanoparticles Concentration	Results
Present study Single basin passive SSs,	Wuhan, China, Latitude (29°58′N and 113°53′E)	Graphite micro-flakes with size 1.3 μm length, 100 nm width and copper oxide with size 1 μm	1% Concentration	– The diurnal yield of the improved still was increased by 41.18% and 32.35% for graphite and CuO nanofluids, respectively, compared with the classical still. – The diurnal exergy efficiencies of MSSs were 4.32% and 3.78% for graphite and CuO nanofluids, respectively, while exergy efficiency for CSS was 2.63%. – HTCs and exergy destruction in still the components with and without nano-micro particles was evaluated.
Sahota et al. [16] ADSSS integrated with N- (PVT) and water FPC	New Delhi, India, Latitude (28°38′N and 77°13′E)	CuO nanoparticles size 20 nm	The best concentration (0.131%)	The daily fresh water output was 11.45 L for CuO nanofluid.
Gupta et al. [28]. Single basin active SS	Jabalpur, India, Latitude (23°10′N and 79°59′E)	Not given	0.12%, Only one concentration	Using CuO improves the productivity by approximately 22.42% and 30.072% at brine depths of 5 cm and 10 cm, respectively, compared with CSS.
Sahota and Tiwari [29] Passive, DSSS	New Delhi, India Latitude (28°38′N and 77°13′E)	CuO nanoparticles size 20 nm	0.2, 0.25 and 0.3% The best concentration was 0.25%.	The best energy efficiency gained for CuO nanofluid was 43.81%, while the pure water was 37.78%.
Sahota et al. [30] Active DSSS	New Delhi, India, Latitude (28°38′N and 77°13′ E)	CuO nanoparticles size 20 nm	Only one concentration 0.25%	Using CuO with heat exchanger in the basin enhanced the freshwater output by about 31.49%, compared with the pure water.

Table 5
Price of different components of fabricated solar stills.

Items	Classical still	Solar still with copper	Solar still with graphite
Fabrication setup	400	400	400
Glass cover	13	13	13
Paints and silicon	10	10	10
Insulation	20	20	20
Ducts and hoses	10	10	10
Micro particles	0	60	120
Total fixed costs (F)	453 RMB	513 RMB	573 RMB

and CSS, respectively.

Acknowledgment

N.Y. was sponsored by National Natural Science Foundation of China (No. 51576076 and No. 51711540031), Hubei Provincial Natural Science Foundation of China (2017CFA046) and Fundamental Research Funds for the Central Universities (2016YXZD006). The authors thank the National Supercomputing Center in Tianjin (NSCC-TJ) and China Scientific Computing Grid (ScGrid) for providing assistance in computations.

References

[1] Velmurugan V, Gopalakrishnan M, Raghu R, Srithar K. Single basin solar still with fin for enhancing productivity. Energy Convers Manage 2008;49:2602–8.
[2] Elshamy SM, El-Said EMS. Comparative study based on thermal, exergetic and economic analyses of a tubular solar still with semi-circular corrugated absorber. J Clean Prod 2018;195:328–39.
[3] El-Agouz SA. Experimental investigation of stepped solar still with continuous water circulation. Energy Convers Manage 2014;86:186–93.
[4] Saadi Z, Rahmani A, Lachtar S, Soualmi H. Performance evaluation of a new stepped solar still under the desert climatic conditions. Energy Convers Manage 2018;171:1749–60.
[5] Sarhaddi F, Farshchi Tabrizi F, Aghaei Zoori H, Mousavi SAHS. Comparative study of two weir type cascade solar stills with and without PCM storage using energy and exergy analysis. Energy Convers Manage 2017;133:97–109.
[6] Sharshir S, Peng G, Yang N, Eltawil MA, Ali MKA, Kabeel A. A hybrid desalination system using humidification-dehumidification and solar stills integrated with evacuated solar water heater. Energy Convers Manage 2016;124:287–96.
[7] Samuel DH, Nagarajan P, Sathyamurthy R, El-Agouz S, Kannan E. Improving the yield of fresh water in conventional solar still using low cost energy storage material. Energy Convers Manage 2016;112:125–34.
[8] Kumar S, Tiwari A. Design, fabrication and performance of a hybrid photovoltaic/thermal (PV/T) active solar still. Energy Convers Manage 2010;51:1219–29.
[9] Xie G, Xiong J, Liu H, Xu B, Zheng H, Yang Y. Experimental and numerical investigation on a novel solar still with vertical ripple surface. Energy Convers Manage 2015;98:151–60.
[10] Singh D, Tiwari G. Exergoeconomic, enviroeconomic and productivity analyses of basin type solar stills by incorporating N identical PVT compound parabolic concentrator collectors: a comparative study. Energy Convers Manage 2017;135:129–47.
[11] Joshi P, Tiwari G. Energy matrices, exergo-economic and enviro-economic analysis of an active single slope solar still integrated with a heat exchanger: a comparative study. Desalination 2018;443:85–98.
[12] Elango T, Kannan A, Kalidasa Murugavel K. Performance study on single basin single slope solar still with different water nanofluids. Desalination 2015;360:45–51.
[13] Kabeel A, Omara Z, Essa F. Improving the performance of solar still by using nanofluids and providing vacuum. Energy Convers Manage 2014;86:268–74.
[14] Sahota L, Tiwari GN. Effect of Al2O3 nanoparticles on the performance of passive double slope solar still. Sol Energy 2016;130:260–72.
[15] Sharshir SW, Peng G, Wu L, Yang N, Essa FA, Elsheikh AH, et al. Enhancing the solar still performance using nanofluids and glass cover cooling: experimental study. Appl Therm Eng 2017;113:684–93.
[16] Sahota L, Gupta VS, Tiwari GN. Analytical study of thermo-physical performance of nanofluid loaded hybrid double slope solar still. J Heat Transfer 2018;140:112404–14.
[17] Sharshir SW, Elsheikh AH, Peng G, Yang N, El-Samadony MOA, Kabeel AE. Thermal performance and exergy analysis of solar stills – a review. Renew Sustain Energy Rev 2017;73:521–44.
[18] Dwivedi VK, Tiwari GN. Experimental validation of thermal model of a double slope active solar still under natural circulation mode. Desalination 2010;250:49–55.
[19] Vaithilingam S, Esakkimuthu GS. Energy and exergy analysis of single slope passive solar still: an experimental investigation. Desalin Water Treat 2015;55:1433–44.

[20] Ranjan KR, Kaushik SC, Panwar NL. Energy and exergy analysis of passive solar distillation systems. Int J Low-Carbon Technol 2013.
[21] Tiwari GN, Dimri V, Chel A. Parametric study of an active and passive solar distillation system: energy and exergy analysis. Desalination 2009;242:1–18.
[22] Sharshir SW, Peng G, Wu L, Essa FA, Kabeel AE, Yang N. The effects of flake graphite nanoparticles, phase change material, and film cooling on the solar still performance. Appl Energy 2017;191:358–66.
[23] Velmurugan V, Deenadayalan C, Vinod H, Srithar K. Desalination of effluent using fin type solar still. Energy 2008;33:1719–27.
[24] Tchinda R, Kaptouom E, Njomo D. Heat and mass transfer processes in a solar still with an indirect evaporator–condenser. Energy Convers Manage 2000;41:93–107.
[25] Heris SZ, Etemad SG, Esfahany MN. Convective heat transfer of a Cu/water nanofluid flowing through a circular tube. Exp Heat Transf 2009;22:217–27.
[26] Vajjha RS, Das DK. Experimental determination of thermal conductivity of three nanofluids and development of new correlations. Int J Heat Mass Transf 2009;52:4675–82.
[27] Aghaei Zoori H, Farshchi Tabrizi F, Sarhaddi F, Heshmatnezhad F. Comparison between energy and exergy efficiencies in a weir type cascade solar still. Desalination 2013;325:113–21.
[28] Gupta B, Shankar P, Sharma R, Baredar P. Performance enhancement using nano particles in modified passive solar still. Procedia Technol 2016;25:1209–16.
[29] Sahota L, Tiwari GN. Effect of nanofluids on the performance of passive double slope solar still: a comparative study using characteristic curve. Desalination 2016;388:9–21.
[30] Sahota L, Shyam, Tiwari GN. Analytical characteristic equation of nanofluid loaded active double slope solar still coupled with helically coiled heat exchanger. Energy Convers Manage 2017;135:308–26.
[31] Omara ZM, Eltawil MA, ElNashar EA. A new hybrid desalination system using wicks/solar still and evacuated solar water heater. Desalination 2013;325:56–64.